Evidence of active tectonics in the Augusta Basin (eastern Sicily, Italy) by Chirp sub-bottom sonar investigation

Claudia Pirrotta[1,*], Maria Serafina Barbano[1], Daniela Pantosti[2], Paolo Marco De Martini[2]

[1] *Università di Catania, Dipartimento di Scienze Biologiche, Geologiche e Ambientali, Catania, Italy*

[2] *Istituto Nazionale di Geofisica e Vulcanologia, Sezione Roma 1, Rome, Italy*

ABSTRACT

*A Chirp sub-bottom sonar investigation was performed in the 150 km²
wide Augusta Basin, located offshore eastern Sicily, a region repeatedly hit
by strong earthquakes in historical time, with the end of identifying pos-
sible evidence of active tectonics. Seismostratigraphy shows two main re-
flectors: R1, which represents the Last Glacial Maximum erosional
surface, formed between 60 ka and 19 ka BP, and R2 that is the top of the
Holocene deposits. Morphobathymetry reveals two marine abrasion sur-
faces, Ms1 and Ms2 that are related to the 35 ka and 25 ka BP marine high
stills, respectively. R1 surface and the onlapping Holocene sediments are
affected by normal and probably strike-slip faulting. The oldest NE-SW
striking normal fault system dislocates R1 surface but not the Holocene
deposit. NNW-SSE striking extensional faults show more recent activity
since they displace Ms2 abrasion surface, the Holocene sequence and cause
seafloor up-warping. NE-SW normal faults produce asymmetric basins
where the Holocene deposits form wedged bodies. ENE-WSW left-lateral
faults dissect a paleo-island, Ms2 and the NNW-SSE fault system. More-
over, seismically induced slumps involving the Holocene sediments, are
found at the foot of some fault scarps. The presence of slumped bodies
and active faults indicates ongoing deformation in the basin. Identified ac-
tive faults are consistent with the main regional Malta Escarpment fault
system, of which they can be considered as the incipient westernmost ex-
tension. This study supports the hypothesis that the Malta Escarpment is
active and can be responsible for the regional seismicity.*

1. Introduction

The coastal area of south eastern Sicily experi-
enced several large magnitude earthquakes and
tsunamis in pre-instrumental times (Figure 1) [CPTI
Working Group 2004]. The location of the historical
earthquakes is only based on macroseismic data and
Pleistocene-Holocene evidence for tectonic activity of
the region reported in the geological literature is lim-
ited and ambiguous. This is because the focus of most

published papers has a broader scale, the data on re-
cent deposits are scant and the probable location off-
shore of the seismogenic faults has been hindered by
insufficient marine data from the near shore. There-
fore an open debate exists on the seismotectonic set-
ting of this region and in particular on the question of
whether the sources of the strong events (e.g. the 1169
and 1693 earthquakes) are located inland and associ-
ated with known Quaternary faults [e.g. Visini et al.
2009 and references therein], or located offshore and
linked to the NNW-SSE striking Malta Escarpment
fault system (MEF in Figure 1) [e.g. Bianca et al. 1999,
Azzaro and Barbano 2000] or to the NW-SE trending
transtensive fault (STEP Fault, SF in Figure 1) located
at about 70 km to the E of the Malta escarpment, as
recently suggested by Polonia et al. [2011].

This work focuses on the Augusta Basin (Figure
1), located in the Ionian offshore, north-east of the Hy-
blean Foreland, which is considered a key area to clar-
ify the seismotectonic setting of eastern Sicily. For this
reason, we performed a geophysical survey using high-
resolution sub-bottom Chirp techniques, which are
particularly suited to this kind of study. Indeed, al-
though the signal penetration is generally limited, its
resolution is excellent and produces seismic images dis-
playing recent and shallow sedimentary and tectonic
structures. Moreover, it allows investigating shallow
water environments, as is the case of the Augusta
Basin, and offers the possibility of exploring a contin-
uous and well preserved offshore sedimentary record
with a detail comparable to inland outcrop observa-
tions. In recent applications, Chirp sub-bottom analy-
sis performed in several basins worldwide has
highlighted submarine slides, soft sediment deforma-

tions, slumps and active faults that affect young deposits, as well as revealing the tectonic control and seismicity in the examined region [Bull et al. 2006, Dingler et al. 2009, Rebesco et al. 2009, Le Dantec et al. 2010, Doughty et al. 2010, Polonia et al. 2011].

With the aim of evaluating the morphobathymetry of the Augusta Basin and identifying possible evidence of active tectonics, 22 Chirp profiles (for a total length of about 180 km) have been analyzed.

2. Seismotectonic setting

Eastern Sicily is located along the African-Eurasia boundary [Dewey et al. 1989] where, in response to the NNW–SSE orientated convergence between Africa and Europe, the southeastern-verging Apenninic-Maghrebian Thrust Belt is emplaced on the Pelagian continental crust. The culmination of the Pelagian Block in the southeastern sector of Sicily is represented by the Hyblean foreland , whose present geometry is the result of the Neogene-Quaternary flexure beneath the orogenic belt, which caused the development of NE-SW oriented en-echelon faults and Quaternary extensional basins [Lentini and Vezzani 1978]. Eastward, the Hyblean foreland confines with the Ionian Basin, the last remaining segment of oceanic crust of the central Mediterranean bending below the Apenninic-Maghrebian Thrust Belt in correspondence of the Calabrian Arc (CA). The separation between the Hyblean Foreland and the Ionian Basin occurs by the Malta–Escarpment Fault System (MEF) (Figure 1), a NNW-SSE trending E dipping fault belt with ~ E-W and ENE-WSW associated structures [Finetti and Del Ben 1996, Bianca et al. 1999], running for some hundreds of kilometres from the north African coast up to the mid-Ionian coast of Sicily [Scandone et al. 1981]. According to some authors, MEF belongs to an incipient rifting system affecting Calabria and eastern Sicily [Monaco and Tortorici 2000], although recent seismic line interpretation [Argnani et al. 2013] shows that it does not continue north of Catania but is offset eastward. On the contrary, other authors [i.e. Palano et al. 2012 and references therein] consider MEF as the southern prosecution of the transtensive Aeolian Tindari Letojanni Fault (ATLF) system (Figure 1). This system has been interpreted either as a transfer crustal zone between the CA thrust belt, located in the northern Sicily offshore, and the accretionary wedge, in the southeastern Calabria offshore, or as a lithospheric boundary between the Hyblean foreland and Ionian blocks accommodating different rates of Ionian slab roll back [e.g. Doglioni et al. 2007, Chiarabba et al. 2008].

The active tectonics characterizing southeastern Sicily is also associated with frequent seismicity. During

historical times several strong earthquakes (1169, M = 6.6; January 9 and January 11, 1693, M = 6.2 and M = 7.4, respectively; CPTI Working Group [2004]) struck the region (Figure 1) and produced disastrous tsunamis. Definitive seismogenic source assignation is difficult for incomplete record of damage distribution. Indeed the 1169 event is based on very poor evidence and historical data may be misleading for the January 11, 1693, main shock, since damage related to this event results from the cumulative effects [Azzaro and Barbano 2000] of at least two large shocks (January 9 and 11). According to some authors, the sources of these earthquakes are within the set of Quaternary faults observed inland [Visini et al. 2009 and references therein], thus large submarine landslides are suggested to have caused the tsunamis [e.g. Billi et al. 2010, Di Bucci et al. 2010, and references therein].

Other authors, taking into account earthquake related tsunamis and the lack of surface faulting evidence inland, agree in locating the sources of these events off-
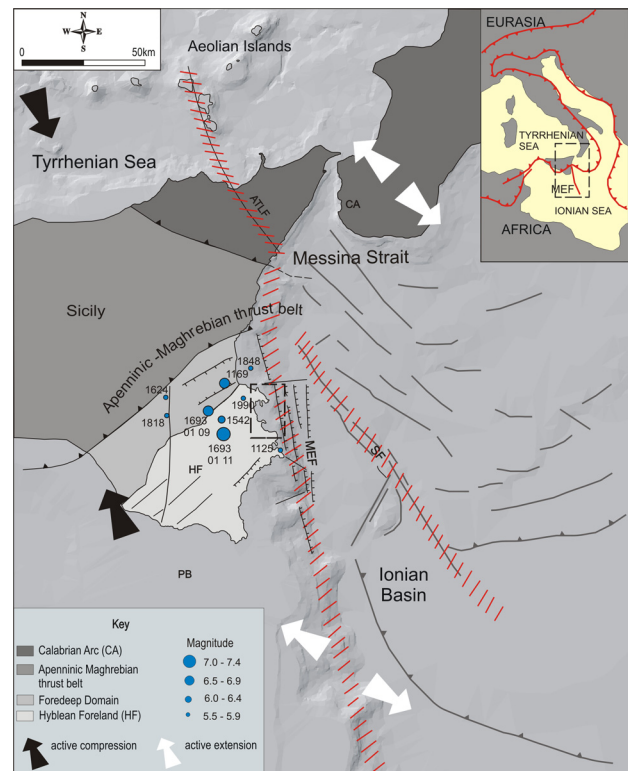

Figure 1. Structural map of eastern Sicily showing the main domains and structural elements: the Apenninic-Maghrebian Thrust Belt, the Hyblean Foreland (HF) affected by faults and bounded by the Malta Escarpment (MEF) connecting HF to the Ionian Basin. Circles are the epicentres of the strong historical earthquakes [CPTI Working Group 2004]; arrows indicate active contraction and extension (modified from Palano et al. 2012); dashed lines are the two belts of active deformation of the Ionian Sea proposed by Palano et al. [2012]: MEF and the STEP Fault (SF) according to Polonia et al. [2011]; the dashed line rectangle delimits the Augusta Bay shown in Figure 2. Inset shows the Africa-Eurasia plate configuration, rectangle shows the location of Figure 1.

shore, in association with the Malta Escarpment System [e.g. Azzaro and Barbano 2000, Monaco and Tortorici 2000, Argnani and Bonazzi 2005]. For a complete review of the proposed seismogenic sources refer to the Database of Individual Seismogenic Sources, DISS [Basili et al. 2008, DISS working group 2010]. Recently, Polonia et al. [2011, 2012] proposed a new source located in the Ionian Sea: the STEP fault system, a system of out of sequence thrusts (splay faults) at the rear of the accretionary wedge (Figure 1).

The Augusta area was also hit by moderate earthquakes in the past. The December 1542 (M = 6.6) and the January 11, 1848, (M = 5.5) events occurred in pre-instrumental times and their sources were then only approximately located nearby the Augusta harbour [CPTI Working Group 2004]. The epicentral location of the

62° north-dipping conjugate plane.

The analysis of earthquakes recorded from 1994 to 2002 in southeastern Sicily [Musumeci et al. 2005, Brancato et al. 2009] and focal mechanisms of events with magnitude > 3.0, located along the Ionian coast, have shown that strike-slip and normal mechanisms were predominant and that only 10% of the earthquakes show inverse focal solutions. However, the overview of seismic activity and faulting inland and offshore of the Hyblean foreland testifies to a complex seismotectonic regime with σ_1 oriented NNW-SSE and σ_3 oriented ENE-WSW [Palano et al. 2012 and reference therein]. This scenario should indicate normal faulting coupled with dextral mechanisms along the NNW-SSE faults and left-lateral component along the ~ E-W and ENE-WSW faults of the MEF system.
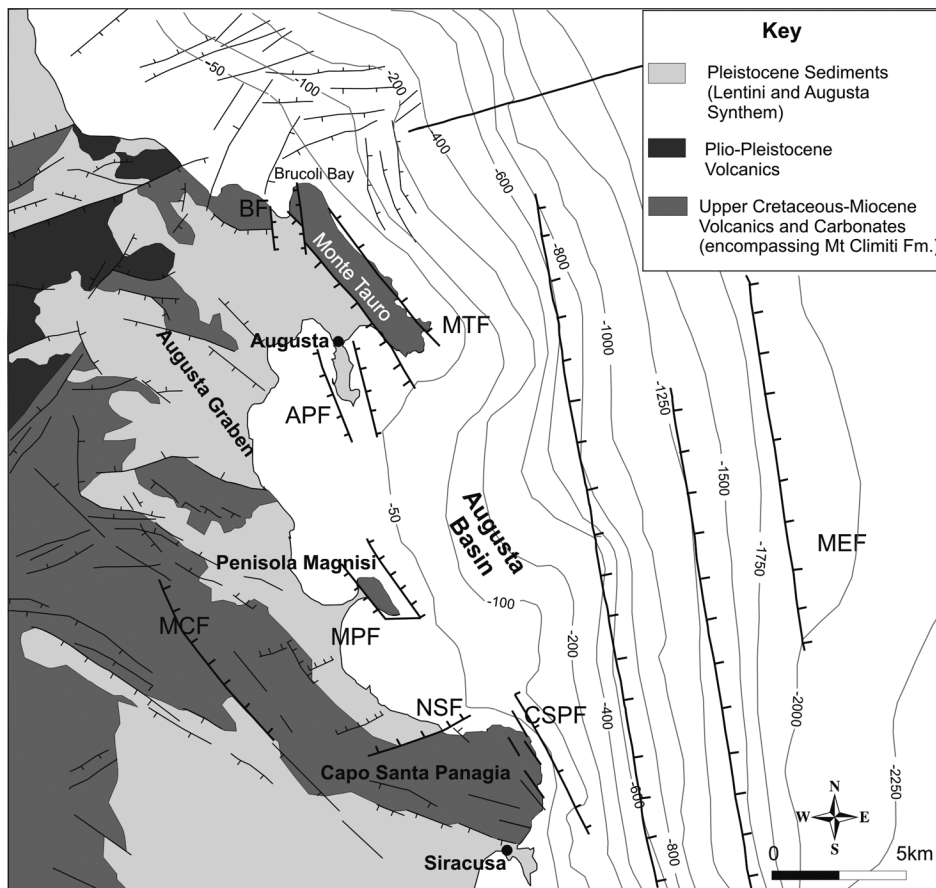
Figure 2. Geological sketch map of Augusta Graben showing the emerged Augusta Bay and the actual Augusta Basin. Structural elements are from: Ambrosetti et al. [1987], Catalano et al. [2010] and Carbone et al. [2011]; BF = Brucoli Faults; MTF = Mt Tauro Faults; APF = Augusta Peninsula Faults; MCF = Mt Climiti Fault; MPF = Magnisi Peninsula Faults; NSF = North Siracusa Fault; CSPF= Capo Santa Panagia Faults; MEF = Malta Escarpment Fault.

December 13, 1990, event (M = 5.5) and its aftershock (M = 4.2) the December 16, 1990, are well defined near the coast of Augusta (Figure 1). According to a first model [Amato et al. 1995], the fault-plane solution of the 1990 main shock suggests either left-lateral motion on a NS vertical plane or a right lateral one on the E-W,
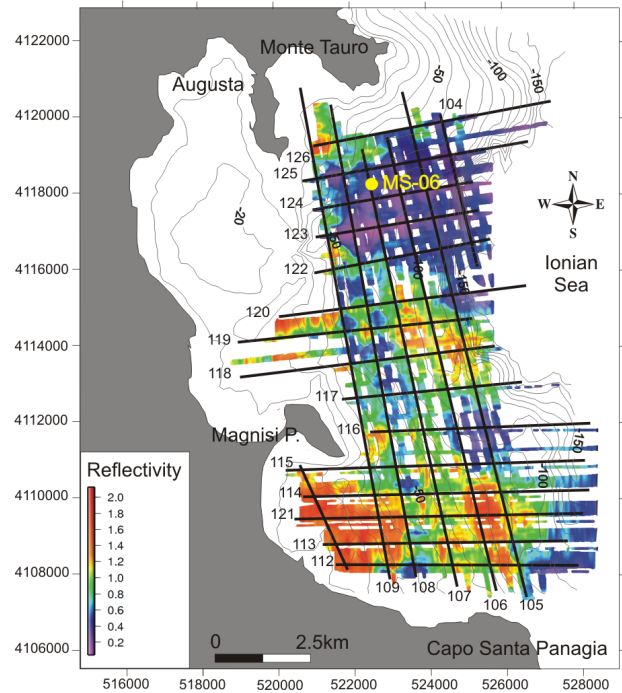
2.1. The Augusta Bay

The north-eastern edge of the Hyblean foreland comprises a complex network of NW-SE, NNW-SSE, NE–SW and ~ ENE-WSW faults that bound structural highs and extensional basins filled by Quaternary deposits, among which the widest is the NW-SE ori-

ented Augusta Graben (Figure 2).

The Augusta Graben comprises an emerged sector and the present-day Augusta Basin to the east, representing a NNW-SSE trending tectonic low. The current setting of the Augusta Graben originates from the activity of bounding Quaternary faults that are visible inland, some of them probably extend offshore (Figure 2). In the northern sector of the Graben, NW-SE faults border the Monte Tauro Horst (MTF in Figure 2). The 15 km-long, N150°E-striking and NE-dipping Mt. Climiti Fault [Bianca et al. 1999] delimits the Graben to the west (MCF in Figure 2). The almost E-W oriented N-dipping North Siracusa Fault (NSF in Figure 2) [Catalano et al. 2010] bounds the southern margin of the Graben. Other minor NNW-SSE faults bound the Brucoli Bay (BF in Figure 2) and the Augusta (Augusta Peninsula Faults, APF in Figure 2) and Magnisi Peninsulas (Magnisi Peninsula Faults, MPF in Figure 2) [Carbone et al. 2011]. Another set of NNW-SSE, ENE dipping faults crop out in the area of Capo Santa Panagia, both inland and offshore [Adam et al. 2000] (CSPF in Figure 2).

These faults affect terrains mainly consisting of Miocene limestones (Mt Climiti Fmt.; Carbone et al. [2011]) discordantly overlapped by Middle-Upper Pleistocene marine deposits of littoral to deep water environments (Figure 2) (Lentini and Augusta Synthem; Carbone et al. [2011]). Among these, the NNW-SSE faults show evidence of recent activation, whereas the NW-SE ones seem to be inactive. The Mt. Climiti fault activity is confined to the 850-330 ka interval, since it is crossed by the 330 ka-old undisturbed paleoshoreline [Bianca et al. 1999, Catalano et al. 2010]. Geological and geomorphologic evidence highlights that the NW-SE Monte Tauro faults, characterized by strongly eroded scarps, have not been active since the Pliocene, and their northern section is displaced by the NNW-SSE faults that border the Brucoli Bay (BF in Figure 2) [Carbone et al. 2011]. The NNW-SSE faults belonging to the Malta Escarpment system (MEF in Figure 2) bound the Augusta Basin to the east and seem to be active, as suggested by the analysis of seismic reflection profiles [Bianca et al. 1999]. They caused seafloor faulting and development of sedimentary basins north of Siracusa [Argnani and Bonazzi 2005].

The uplift of the Augusta area due to tectonics and regional bulging has been estimated to be 0.6-0.7 mm/yr, studying the emerged Quaternary paleo-shorelines and marine terraces observed inland along the Mt. Climiti eastern slope [Bianca et al. 1999, Catalano et al. 2010]. In the Augusta area, Di Grande and Scamarda [1973] observed the lower marine terrace at a few metres a.s.l. assigned to the Marine Isotopic Stage (MIS) 3.3 (60 ka) [Catalano et al. 2010].

Figure 3. Chirp sub-bottom seismic profile grid (numbered black lines) and reflectivity map of the Augusta Basin, colour scale indicates different reflectivity values; yellow dot shows location of the long sediment gravity core (MS-06) by Smedile et al. [2011].

3. Method

A dense grid of Chirp sub-bottom sonar profiles was surveyed in the Augusta Basin (Figure 3) during a cruise made in Summer 2007, within a cooperation program between INGV (Istituto Nazionale di Geofisica e Vulcanologia, Italy), the Geological Department of the Catania University and CNR-ISMAR (Istituto di Scienze Marine, Italy). Geophysical data were acquired using a deep-towed Chirp-sonar (Datasonics SIS-1000) operating at a frequency of 3-7 kHz. The instrument was also fitted with an ADSL link from the tow-fish to the topside computers. The deployment configuration was complemented with an onboard motion sensor and a global positioning system (GPS) receiver to measure real position for every shot. The surveyed grid covers an area of 90 km^2 and consists of 22 lines striking ~N-S and ~E-W, for a total length of 180 km (Figure 3), an average line spacing of 1 km with a 0.45 m shot interval.

Processing included the following steps: data conversion to standard SEGY format, semi-automatic picking function, correction, amplitude gain and display using the SeisPrho software package [Gasperini and Stanghellini 2009]. Two-way travel-times were converted to depth assuming a water velocity of 1500 m/s. This conversion provides an acceptable representation of the sea bottom and a minimum value of the sediment thicknesses in metres. The acoustic reflectors identified in the profiles were digitized and mapped.

Reflectivity values were automatically obtained (Figure 3) by analyzing amplitudes of source vs. reflected signals [Gasperini and Stanghellini 2009]. Reflectivity and morphobathymetry maps were then generated through contouring software (Surfer 8.0, Surface Mapping System, Copyright 1993, 2002, Golden Software, Inc). Low reflectivity values, approaching to zero, are indicative of deposits with fine grain size, on the contrary values approaching to 2 are typical of coarse deposits. Also, sediment package that appears transparent in the chirp profile image is either a loose or weakly cemented deposit, while a well cemented deposit does not allow the signal penetration below its surface.

4. Chirp profile study

4.1. Seismostratigraphy

Seismic Chirp profiles show two main reflectors R1 and R2. The deepest reflector, R1 (Figure 4), is characterized by high reflectivity values (between 1 and 1.5) and in many Chirp profiles the signal does not penetrate beneath it, thus in these profiles R1 is interpreted

as the top of the acoustic bedrock (HRF, highest reflectivity facies in Figure 4a). In some profiles beneath the R1 surface, several inclined, eastward prograding reflectors are visible. These are interpreted as belonging to a clinoform facies (CF in Figure 4b) [Firetto Carlino et al. 2012]. Even if the bottom of the clinoform facies cannot be observed, its aspect in Chirp profiles indicates that it is a less cemented deposit with respect to the acoustic bedrock on which it lies. In other Chirp sections, below the R1 surface, a ~10 m thick high amplitude seismic horizon is evident, sometimes it overlays discordantly the clinoform facies. This horizon projects a prolonged echo, has high reflectivity (between 1 and 1.5) and for its features has been interpreted as a coarse deposit [Firetto Carlino et al. 2012] hereinafter named prolonged echo facies (PEF in Figure 4c). The acoustic bedrock, the clinoform facies and the prolonged echo facies are often undistinguishable from each other and their spatial distribution cannot be clearly resolved because of the similar acoustic return. Thus these facies are grouped in a unique unit, the Seismo Unit A and their top surface is indistinctly represented by R1.
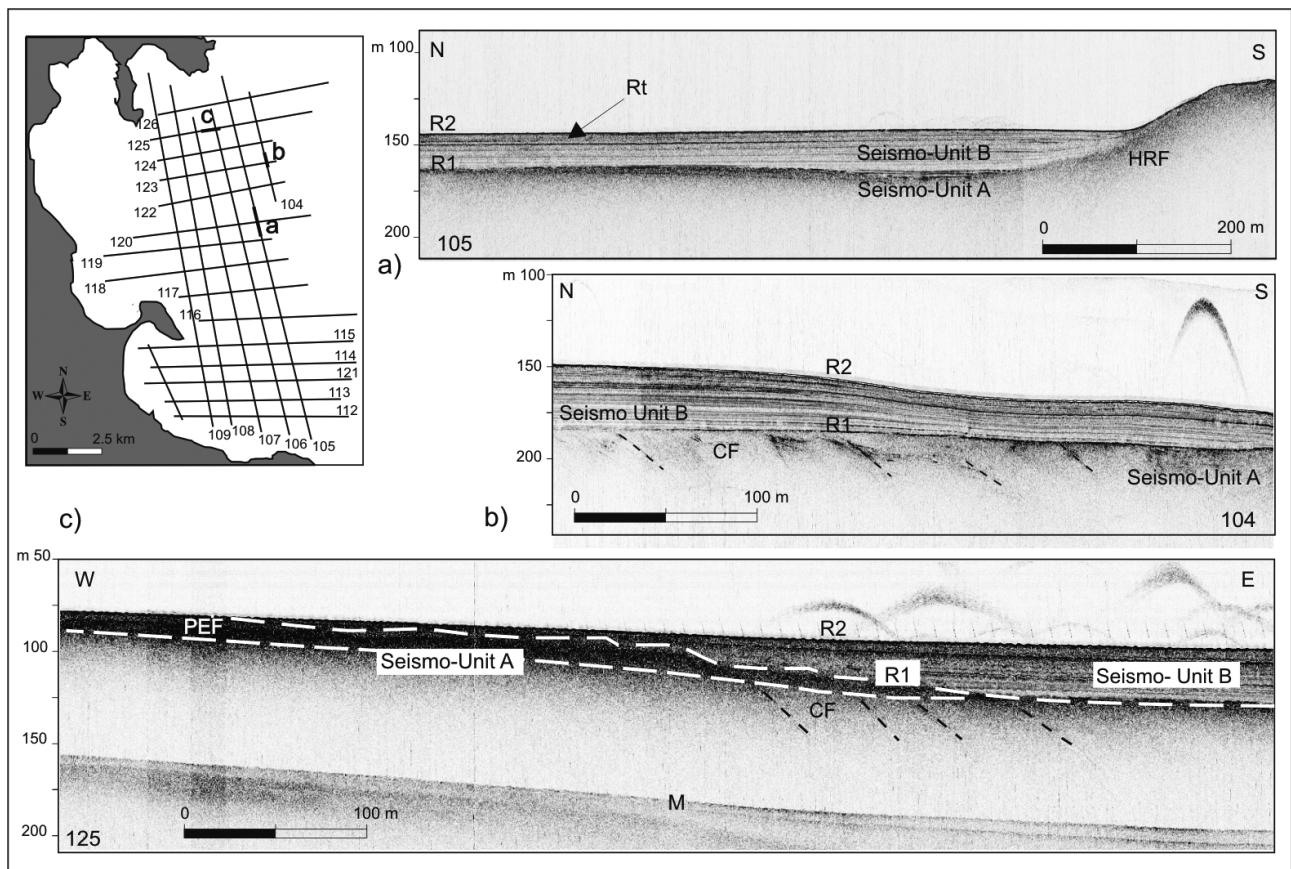
Figure 4. Location of the sections is shown in the profile grid (black lines); seismic lines depicting the seismostratigraphy (the line number is shown at the bottom corners): a) R1 is the main reflector that is the top of the Seismo Unit A here represented by the acoustic bedrock (HRF in the figure); R2 is the top surface of the Seismo Unit B, Rt is the most prominent high-amplitude reflector within the semitransparent sedimentary sequence; note the nearly flat surface echoes of Seismo Unit B layers; b) R1 is the top of the Seismo Unit A here represented by the clinoform facies (CF) on which Seismo Unit B rests; c) in this case R1 is the top of both clinoform facies and prolonged echo facies (PEF), representing Seismo Unit A, onlapped by the Seismo Unit B; M = multiple.
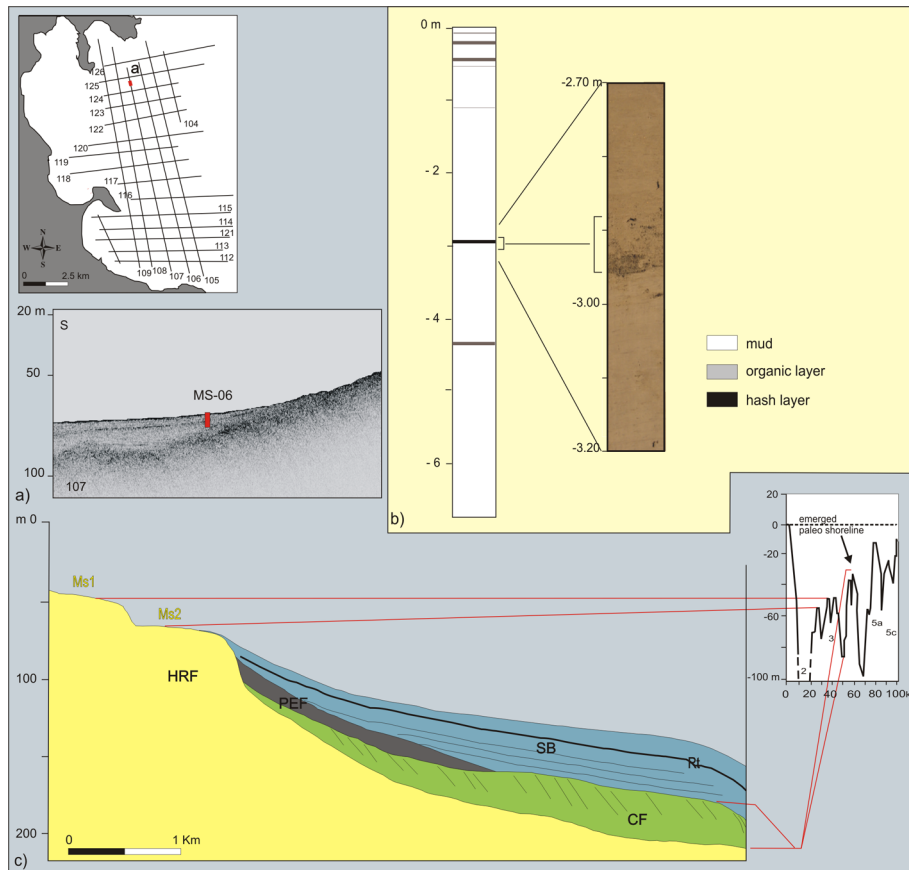
Figure 5. a) Section of profile 107 showing MS-06 sediment core location; b) core stratigraphy reconstruction and detail of the photo showing the ash level sandwiched by mud (modified after Smedile et al. [2011]); c) on the right, sea level oscillation from last 100 ka according to Lajoie et al. [1991]; on the left, correlation with observed features: HRF = highest reflectivity facies, CF = clinoform deposit; PEF = prolonged echo facies, SB = Seismo Unit B; Ms1 = transgressive ravinement surface 35 ka old; Ms2 = transgressive ravinement surface 25 ka old; Rt = high-amplitude reflector within the sedimentary sequence, associated with the 122 BC Plinian Etna eruption [Smedile et al. 2011].

A semitransparent deposit (hereinafter referred as Seismo Unit B) rests unconformably on Seismo Unit A and consists of a homogeneous sequence of sediments with several continuous, parallel internal reflectors, almost horizontally layered and with an aggradational on-lap geometry (Figure 4a,b,c). The top of Seismo Unit B (R2 reflector in Figure 4) has average reflectivity values between 0.1 and 0.6; therefore it is likely made up of a very fine grain size deposit. Minor seismic reflectors observed within the Seismo Unit B suggest the presence of layers characterized by coarse grain-size, alternating with fine (transparent) intervals. A prominent high-amplitude reflector (Rt in Figure 4) (average reflectivity between 0.12 and 0.56) was observed in the northern sector of the basin between 3 m and 10 m b.s. (below seafloor), extending for about 1/3 of the basin area.

A 6.7 m long sediment core (MS-06) was sampled in the Augusta Basin, 2 km offshore at a water depth of 72 m (Figures 3 and 5a) and studied in detail by Smedile et al. [2011]. The core analysis confirms that Seismo Unit B is mainly made up of fine-grained, mud-dominated, sediments and allows correlating reflectivity values with specific layers showing peculiar grain size ranges. Moreover, a 3-4-cm-thick sandy layer, detected in the core at 3 m of depth, can be simply related to the prominent reflector Rt (Figure 5b). This layer consists of a coarse volcanic deposit made of dark fine lapilli and coarse ash that, on the basis of morphoscopic and petrochemical analyses, was associated to the 122 BC Plinian Etna eruption [Smedile et al. 2011]. A depth-age model for the collected core was obtained on the basis of radiocarbon dating, tephrochronology, paleomagnetism and short-lived radionuclides ratios. This model indicates that the MS-06 core sediment sequence records the last 4500 yrs and it is characterized by an average sedimentation rate of about 1.5 mm/yr [Smedile et al. 2011, Sagnotti et al. 2011].

The stratigraphy of the Augusta Basin has been reconstructed combining the seismostratigraphic evidence with data from onshore geology and MS-06 sediment core [Smedile et al. 2011] and also according to the sea level change curve [Lajoie et al. 1991], considering that the youngest marine terrace observed onshore is related to the MIS 3.3 (60 ka) [Catalano et al. 2010].

Given its geophysical characteristics the highest reflectivity facies can be related with the Miocene lime-

stone belonging to the Mt. Climiti Formation and/or to the Pleistocene Lentini and Augusta Synthem [Carbone et al. 2011], locally outcropping inland. Consequently clinoform facies represents a falling stage system tract [Hunt and Tucker 1992] due to the fast re-

Therefore, these surfaces can be associated to the 35 ka BP and 25 ka BP high stills (Figure 5c), also considering that the terrace related to MIS 3.3 (60 ka) was observed inland a few metres above sea level [Catalano et al. 2010]. Due to its position in the chirp profiles, the
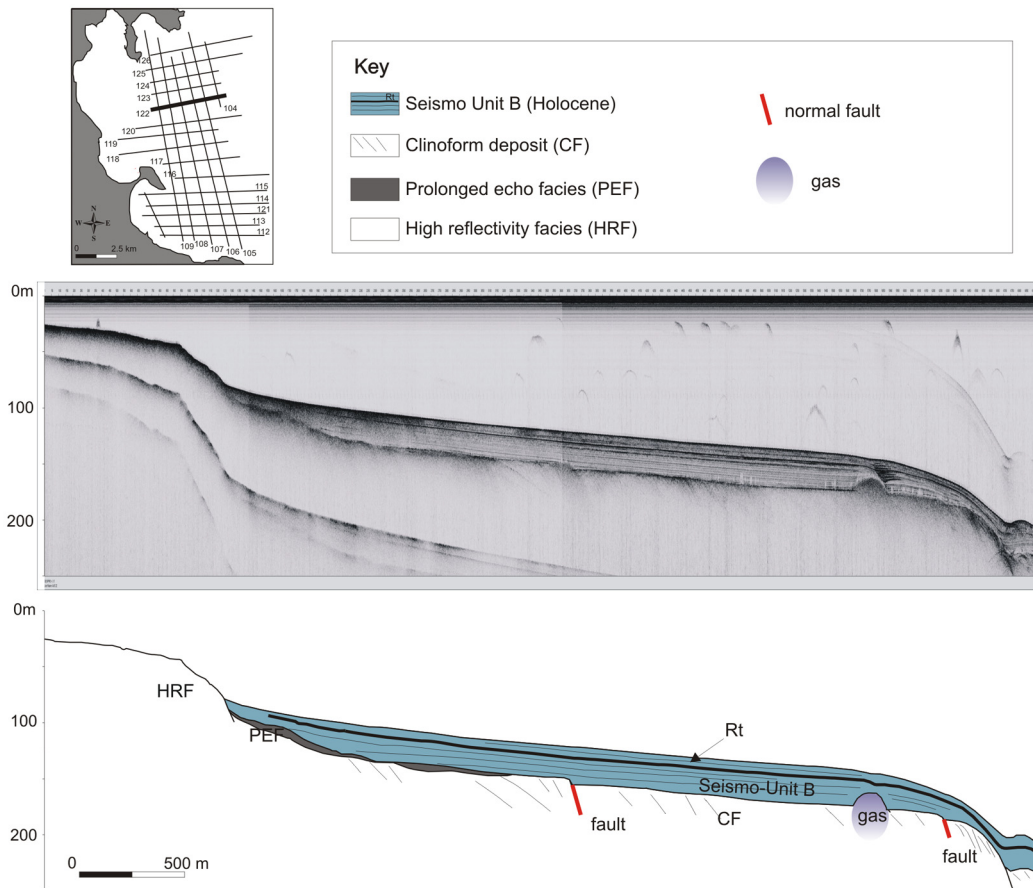

Figure 6. Chirp profile 122 showing the main Augusta basin features and their seismo-stratigraphic relationship.

gressive phase occurring after the highstand at 60 ka BP and culminating at 50 ka BP (Figure 5c).

Thus the top surface of the clinoform facies is the subaerial erosion surface marking the end of the 60-50 ka old regressive phase. The prolonged echo facies can be interpreted as a beach facies of transgressive and highstand systems tract (*sensu* Hunt and Tucker [1992]) [Firetto Carlino et al. 2012] related to one of the highstands occurring after 50 ka (Figure 5c).

Two flat surfaces, Ms1 and Ms2, bordered by few metres high steps, shape Seismo Unit A (Figure 5c). Owing to their morphological features, these surfaces are interpreted as marine transgressive ravinement surfaces [Nummedal and Swift 1987] with their inner/outer edges. Since morphological elements formed by a high stand more easily preserve than that formed by a low stand, given their well preserved status, these two marine abrasion surfaces are associated with two recent marine high stills of which the oldest occurred at a lesser depth than the youngest one.

prolonged echo facies can be related to the transgressive episode producing the youngest abrasion surface (Ms2, 25 ka old).

According to these observations and considering those resulting from MS-06 sediment core analysis, the Seismo Unit B represents the last sedimentary episode corresponding to the Holocene sea level increase. This is confirmed by a rough estimation of the Seismo Unit B age obtained by the sedimentation rate calculated both in the proximal and distal portion of the basin, using as a chronological reference the volcanic ash age (Rt reflector) (122 BC) and its depth below seafloor. In the more proximal sector of the basin, Rt is found at average depth of 3 m b.s.f. and the Seismo Unit B is about 10 m thick. Assuming a constant sedimentation rate, its value is 1,5 mm/yr in this area. Since the deposit below Rt is 7 m thick, it encompasses the last 5 ka, and all the Seismo Unit B package represents the last 7 ka. In the distal part of the northern sector (Figure 6), Seismo Unit B reaches its maximum thickness

(about 35 m) and Rt is found at about 10 m b.s.f. In this area a sedimentation rate of 5 mm/yr can be evaluated, and on this assumption the deposit below Rt is 5 ka old and all the Seismo Unit B seems to record almost the last 7 ka as well.

Therefore the R1 reflector, namely the top of Seismo Unit A and the base of Seismo Unit B, should represent the last erosion phase occurring in the basin, culminating with the Last Glacial Maximum (LGM, 22-19 ka). The hiatus between Last Glacial Maximum erosional surface (R1) and Holocene sedimentary sequence is due to the period of transition from condition of land exposition to that of incipient sea ascent without sedimentation. However, since the Last Glacial Maximum culmination is attested to 22-19 ka BP considering worldwide data, it is likely that in this part of Mediterranean Sea this culmination occurred more recently and the hiatus is shorter.

The reflectivity map (Figure 3) shows considerable variations in reflectivity values and indicates that the seafloor comprises either the acoustic bedrock, clinoform facies and prolonged echo facies or Seismo Unit A reflectors. As a whole, the map shows the lowest reflectivity values in the north-central sector of the Augusta basin, where Seismo Unit B is widely distributed with a maximum thickness of 35 m, while the highest values are found in the southern sector where the Seismo Unit A widely crops out.

4.2. Morphobathymetric analysis

The morphobathymetric maps of the seafloor and acoustic bedrock surface (Figure 7) were obtained by interpolating the R2 and R1 reflectors, respectively.

The map of R1 (Figure 7a) presents the basin conditions at the LGM time. The basin shows a fairly articulated morphology and, on the basis of the morphological characteristics, it can be divided into two highlands in the northern and southern sectors and a morphological low in the central one. The central sector is separated from the north and south highlands by two ENE-WSW parallel morphological lineaments (L1 and L3) and it is also divided into two parts by a further ∼ ENE-WSW lineament (L2). Furthermore a NNW-SSE trending morphological high, bounded by eroded scarps, likely representing a paleo-island (p-I in Figure 7a) is observed at about 6 km from the Magnisi Peninsula.

The Ms1 and Ms2 surfaces and their paleo-shorelines are found at various depths in the different sectors of the basin: at an average depth of −42 m and −63 m respectively in the northern sector (E of the Augusta Peninsula); −51 m and −88 m in the northern part of the central sector; −52 m and −107 m in the southern

part of the central sector, where Ms2 is hidden by the Seismo Unit B; and −49 m and −109 m in the southern sector (SE of the Magnisi Peninsula) (Figure 7).

The present-day seafloor map (Figure 7b) was obtained by combining Chirp data with bathymetry from Nautical Chart from Cape Passero to Cape Santa Croce [Istituto Idrografico della Marina 1999].

The map shows that Seismo Unit B sedimentation occurred mainly in the northern part of central sector with deposits up to 35 m thick and in the narrow and elongated basins near the shore close to the Magnisi Peninsula, with a roughly 10 m thick deposit.

These basins are bordered by aligned scarps, some of them (s1, s2, s3, s4, and s5 in Figure 8a,b,c) appear intensely eroded, while others (f1, f2 and f3 in Figure 8a,b) have steeper slopes and apparently youthful surfaces, not readily associable with the LGM erosive surface.

Even if the Seismo Unit B sedimentation smoothes the basin morphology with respect to that of the pre-LGM basin, a 60 m-high scarp (C-s1) is observed about 7.5 km off the coast (Figure 7b). This scarp represents the easternmost limit of the shelf.
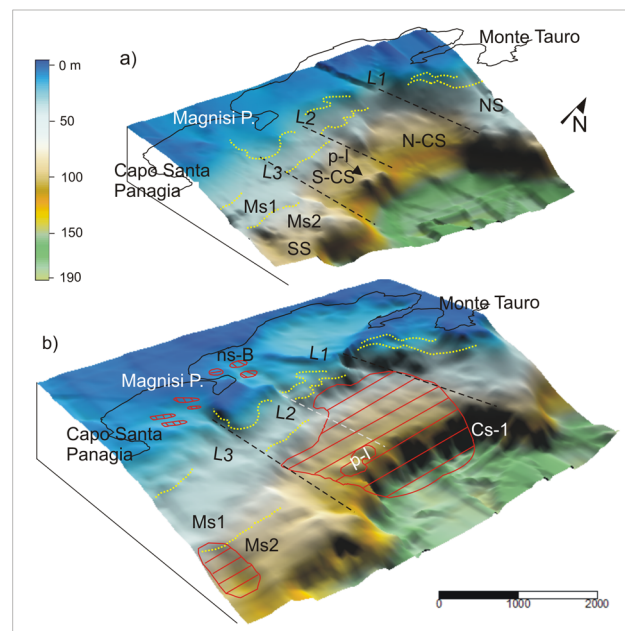
Figure 7. a) DEM of the basin bedrock showing the irregular reflector R1 modified by erosion. The basin can be divided into four sectors: NS = northern sector, N-CS = north-central sector, S-CS = south-central sector, SS = southern sector, separated by L1, L2 and L3; p-I is a paleo-island; Ms1 and Ms2 are two marine abrasion surfaces observed at different depths in the four sectors; dotted yellow lines are the inner edges associated to the abrasion surfaces; b) DEM of the seafloor showing the basin after deposition of the semitransparent Seismo Unit B deposits (delimited by the red contour line) in the north-central and south-central sectors, and in the near shore basins (ns-B) close to the Magnisi Peninsula, C-s1 is the most prominent scarp marking the easternmost limit of the shelf. Vertical exaggeration 3x, scale in metres.
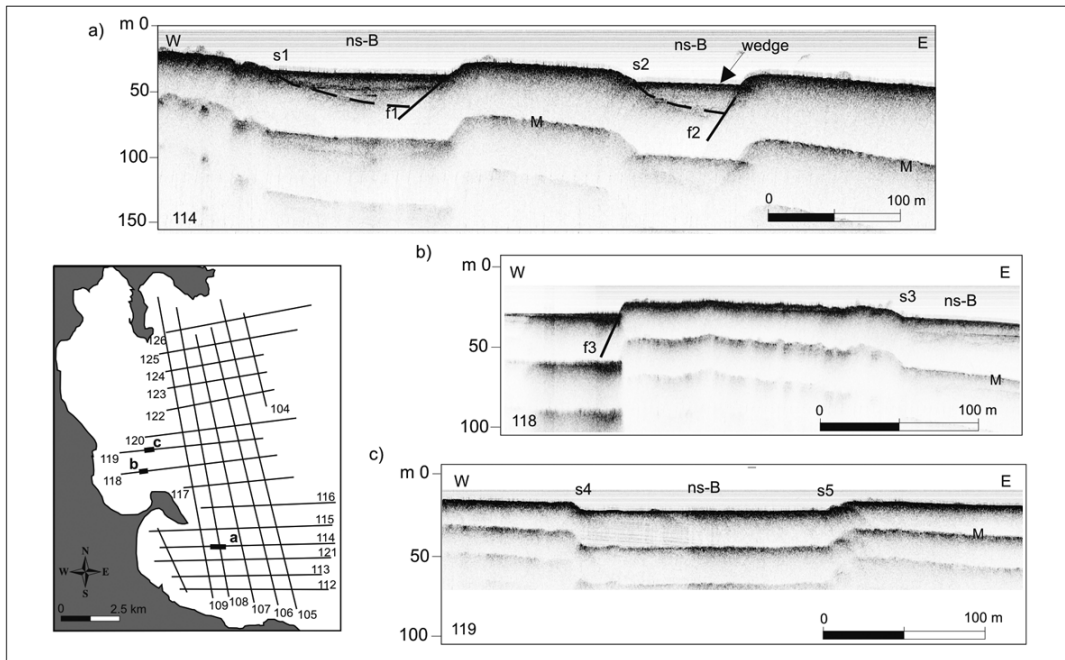
Figure 8. Location of the sections is shown in the profile grid (thick line), the line number is shown at the bottom corners; a) near shore narrow basins, ns-B, bounded by erosional scarps, s1 and s2, on the western side, and steeper, maybe younger scarps, f1 and f2, on the eastern side; b) physiographic high delimited by a steep scarp to the west (f3) and a more gentle and highly eroded one (s3) to the east; c) basin bounded by two highly eroded, scarps s4 and s5.

4.3. Faulting evidence

The Chirp profile and morphobathymetric analyses highlight the presence of several faults in the basin and allowed reconstructing the structural setting of the area.
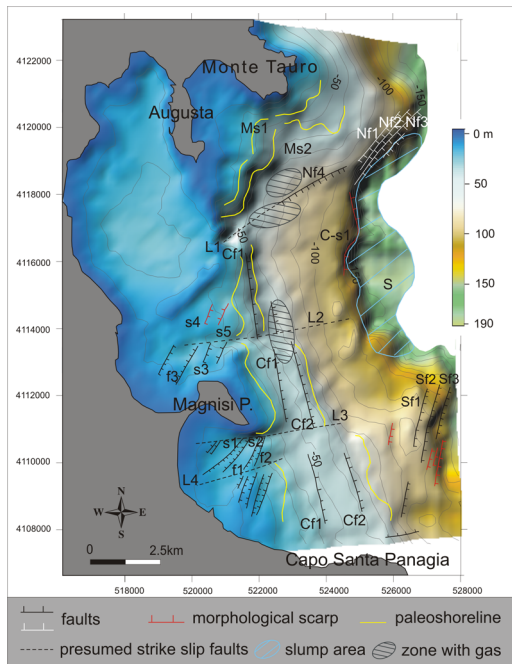
All the faults dislocate R1 surface, modelled from 60 ka up to LGM. However, since R1 coincides with the

Figure 9. Morphobathymetric maps of the seafloor with geomorphologic and structural elements: faults, scarps and paleoshorelines. Faults are represented in both black and white for a better graphic clarity. Dashed lines indicate the morphological lineaments considered strike-slip faults on the basis of the morphological analysis.

top of the clinoform facies (50 ka) in the deepest sector of the basin, where clinoforms are observed, and with the surfaces Ms1 (35 ka) and Ms2 (25 ka) in the shallowest sector, fault age is assigned considering the different age assumed by R1 considering the underlying facies.

In the northern sector NE-SW striking, SE-dipping normal faults (Figure 9) Nf1-2-3 displace R1 by about 40 m of net slip (Figure 10a) whereas the easternmost and most prominent fault Nf3 displaces R1 by 20 m (Table 1). In this sector R1 represents the 50 ky old surface, because below it the clinoform facies is observed (Figure 10a). Seismo Unit B faulting may be apparent because of a mimicking effect of this young loose sediment draping the previously displaced bedrock.

In the same sector, Nf4 is a ENE-WSW trending and SSE-dipping normal fault displacing R1 (Figure 10b and 10c). In other sections Nf4 activity is identified by seafloor up-warping and by deformation of the Seismo Unit B semitransparent deposits in the intercepting Chirp profiles. In the northern part of Chirp profile 104, characteristic syn-tectonic growth strata in the hangingwall of Nf4 (Figure 10d), with a thickening from about 25 m up to 40 m, is evident.

Nf4 also coincides with the northern lineament L1, observed by the morphobathymetric analysis, which separates the high northern and low north central sectors. Across Nf4 the two abrasion surfaces Ms1 and Ms2 are found at different depths and in particular Ms1 steps from -42 m, in the northern sector, to -51 m in north central sector, whereas Ms2 steps from -63 to -88 m. The larger Ms2 15 m displacement may be due to the
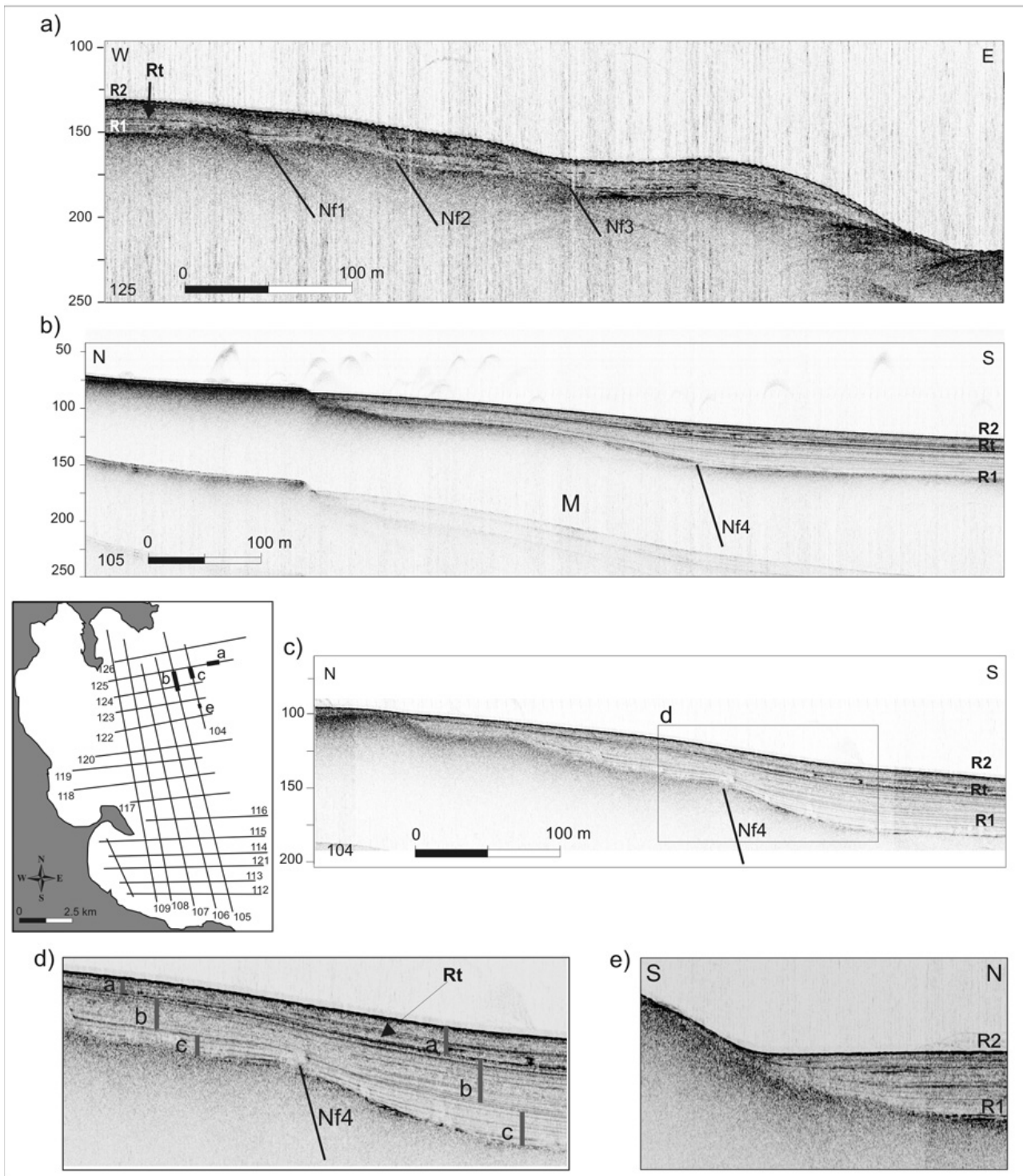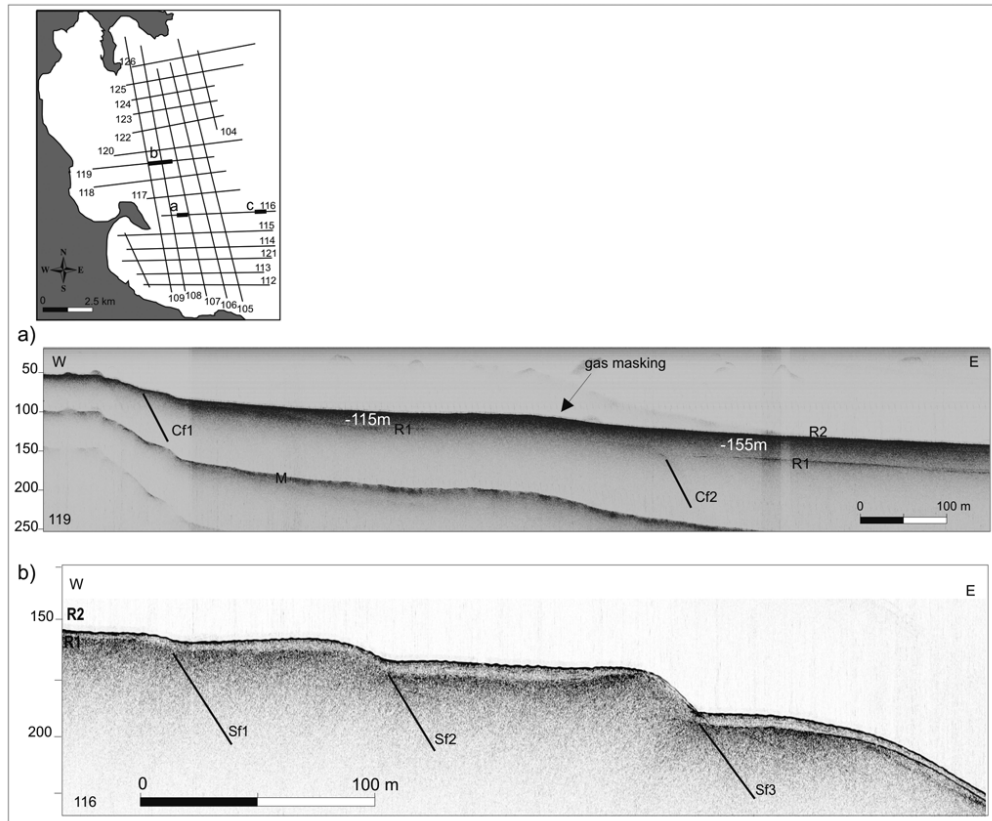
Figure 10. Location of the sections is shown in the profile grid (thick lines); a) 125 Chirp profile located in the northern sector showing the flight of scarps created by normal faults, involving the R1 reflector; b) profile 105 showing Nf4 fault displacing R1; c) scarp coinciding with Nf4 fault affecting R1 reflector; rectangle refers to the blow-up of Figure 10d); d) detail of profile 104 showing probable active deformation of the Seismo Unit B semitransparent deposit; growth strata are imaged in the hangingwall of the Nf4 fault; e) detail of the same 104 Chirp line where strata on-lap the bedrock.

presence of the Cf1 fault, observed as a NNW-SSE trending scarp (Figure 9) in the north central sector.

In the central part of the profile 119 (Figure 11a), R1 surface and Seismo Unit B, are masked by gas that hide the seismostratigraphy. Despite it, a seafloor up-warping can be observed and eastward, beyond the gas cloud, R1 appears at a larger depth than the expected one

(expected depth = −140 m, real depth = −155 m in section 119). This effect is explained by hypothesizing a further NNW-SSE E-dipping, normal fault, Cf2, to the east of Cf1 affecting R1 and Seismo Unit B (Figure 11a). Thus an offset of about 15 m, due to the Cf2 fault activity, can be measured for the R1 surface. Cf2 also causes the displacement of the Ms2 surface of ~ 20 m in the S-CS.

Figure 11. Location of the sections is shown in the profile grid (thick lines); a) R1 reflector displaced by fault Cf2 masked by the gas; numbers refer to depth of R1 surface on the footwall and hangingwall of the fault, M is the multiple; b) flight of scarps created by normal faults in the southern sector involving the R1 reflector below which there is evidence of the clinoform facies (CF).

There, it is found at about −107 m, as a result of cumulative displacement of Cf1 (∼ 15 m) and Cf2.

In the western part of the central sector, NE-SW striking NW dipping normal faults, f1, f2 and f3 delimit the narrow and elongated basins north and south of the Magnisi Peninsula (Figures 8a,b and 9). These faults are responsible for the asymmetry of the small basins, where the thin layers of the Seismo Unit B, form wedged bodies as a consequence of the hangingwall subsidence (Figure 8a).

In the easternmost part of the southern sector, Cf1 and Cf2 faults displace Ms2, which is found at −88 m in the Cf2 footwall, and at −109 m in the hangingwall.

In the southernmost sector, another flight of NNE trending E-SE-dipping normal faults affects the reflector R1 (Sf1-2-3 in Figures 9 and 11b), and the underlying clinoform facies (50 ka old), causing about 38 m of net slip. The easternmost fault (Sf3) shows a vertical offset of about 20 m, whereas the Seismo Unit B largely drapes over the clinoform facies (Figure 11). The ENE-WSW lineament L2 seems to cause left-lateral displacement of Ms1 and Ms2, Cf1 and Cf2, and of the paleo-island (Figure 9), therefore it could be a strike-slip fault. Similarly Cf1 and Cf2 appear to be dislocated further east across the ENE-WSW trending L3 lineament. Finally, L4 lineament could be a further left-lateral fault that delimits the

two sets of the NE-SW trending narrow basins south of the Magnisi Peninsula (Figure 9).

4.4. Soft sediment deformation analysis

In the deepest area of the basin (S in Figure 9), Chirp profiles display the unconsolidated Seismo Unit B sediments that are intensely affected by deformation (Figure 12). Deformed bodies appear as irregular, quasi-hyperbolic chaotic reflectors, showing paucity of coherent internal structure when reflectors are visible. These masses have varying degrees of internal deformation, wave amplitude and height; in general hyperbolic undulations show a maximum amplitude in the order of a hundred metres.

At least two different slumped bodies, named A and B in Figure 12, can be observed in some profiles. The lower body (A) appears more transparent, probably because of the weakening of the acoustic signal (Figure 12); its internal structures can only be partly traced and the bedding is not resolvable since the Chirp signal does not penetrate down to its depth. However, when the deposit stratification is visible, the sedimentary package of the A body appears intensely deformed. The upper body (B) unconformably overlies the lower one (A) and appears less deformed, still preserving the typical Seismo Unit B layering (Figure 12).
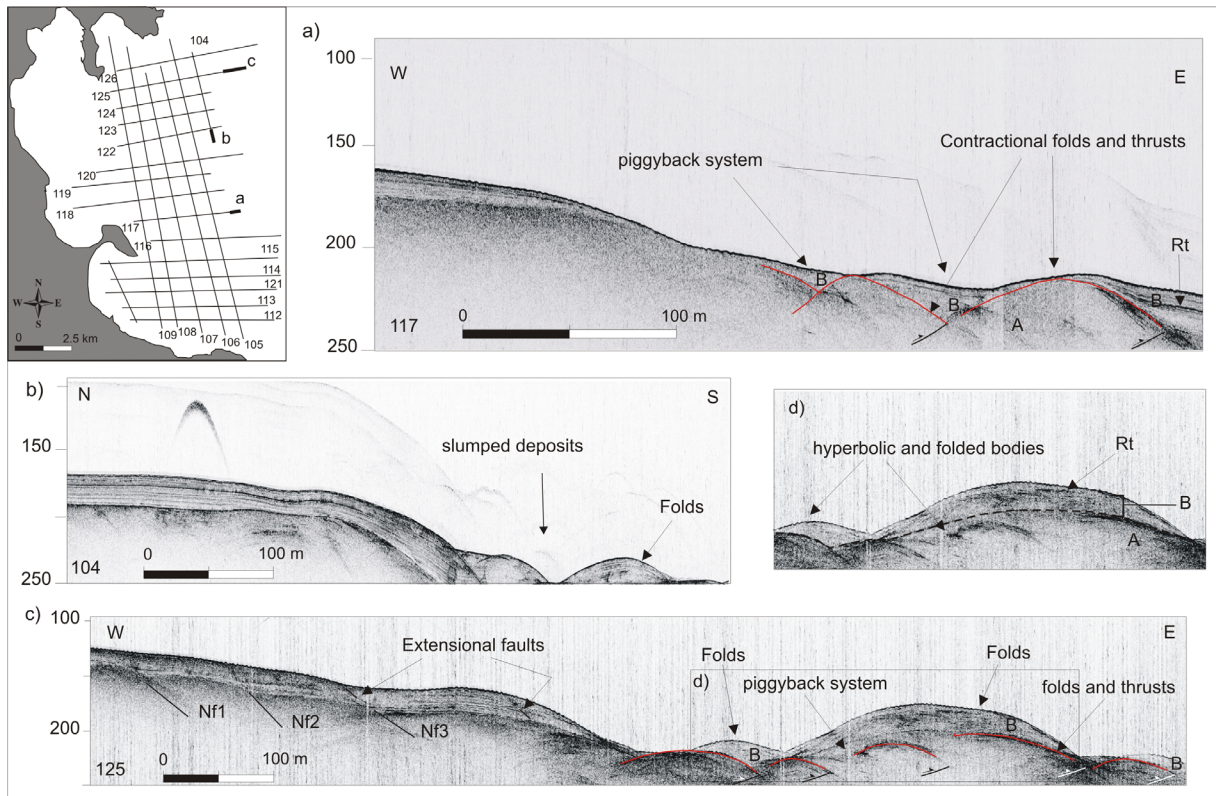
Figure 12. Chirp profiles showing slump accumulations (location of the sections is shown in the profile grid: thick lines. Depth in metres): a) in the south-central sector, close to the L2 fault, slumped masses are observed with contractional folds and thrusts at the toe forming a piggyback system (*sensu* Alsop and Marco [2011]); B body filling the piggyback basins is folded and contains Rt reflector; b) deformation in the north-central sector at the foot of the C-s1 scarp; c) deformation in the northern sector at the foot of the Nf3 scarp; rectangle refers to the detail shown in d; d) detail of the two slumped bodies; please notice the extensional faults at the head of the body and folds at the toe; the lower body A shows more pronounced hyperbolas than the overlying body B.

Within the B body a reflector with the same reflectivity value of the Rt reflector, related to the 122 BC tephra layer, is still recognizable although at different depths.

These deformed bodies show the characteristics of gravity slide masses that typically lie at the toe of scarps and show extensional features at the head and contractional features at the toe. Indeed, little normal faults, observed at the head of the slump indicate gravity-driven extension (Figure 12a) while folds and thrusts, involving the body A, at the toe indicate gravity-driven compression. Also, a piggyback system, which can form in slumped masses due to gravitational thrust propagation [Alsop and Marco 2011], involves A body. The associated piggyback basins are filled by the slumped B body (Figure 12a,c,d).

Unfortunately, Chirp profiles stop at 250 m of depth and cover only the more proximal western side of the deepest area, thus the full extent of the slumps cannot be defined exactly. However, considering only the observed size, the slumps cover an area of almost 20 km^2 (Figure 9) and the body B has an average thickness around 50 m, therefore a minimum volume of ~ 1 km^3 can be evaluated for the upper slump.

The deformed bodies recognized in this area are chaotic and irregular. They do not show basal erosive contact which might suggest a flow energy responsible for transport and deposition. Moreover, sediment accumulation and gravity sliding are located in a narrow and closed inlet, of relatively shallow water (bathymetric range between −120 and −180 m) only 7.5 km away from the shore, at the end of the shelf with no channels and canyons. Thus, effects occurring in marine environment, such as seabottom sediment waves, contour currents or turbidity flows [Doughty et al. 2010 and reference therein], can be excluded as a triggering mechanism. An exceptional trigger, such as earthquake shaking, causing a drop of resistance forces in unconsolidated young deposits, could be responsible for the observed deformational features. On the other hand, slump and slide deposits near branches of active faults have been observed worldwide [e.g. Carter 2012 and reference therein].

Given the different deformational degree, styles and shapes of A and B slumps and their unconformable setting, these two bodies should be related to at least two different deformational episodes. The older body, A, marks the first deformation episode occurring before the Rt deposition, whereas the latter slumped body, B, encompassing the tephra layer, indicates that the deformational event occurred after 122 BC.

5. Discussion

Seismic Chirp profile and bathymetry analyses allowed observing faulting and soft sediment deformation affecting the Augusta Basin.

NNW-SSE and NE-SW faults show normal dip slip kinematics (Figure 9), and affect R1 (60-19 ka erosive surface) and Seismo Unit A. For some of these faults, possible involvement of both marine abrasion surfaces, Ms1 (35 ka) and Ms2 (25 ka), and Holocene deposit (Seismo Unit B) is found too.

ENE-WSW trending lineaments could be left-lateral faults dislocating the NNW-SSE Cf1 and Cf2 faults, the marine abrasion surfaces Ms1 and Ms2 and the paleo-island.

Table 1 summarises parameters of the detected faults, inferred age, vertical displacement of the normal faults and the slip rate when it can be calculated. However, since the slip rate varies both along fault segments and temporally, particularly where fault segments interact, assessed values should be considered approximate.

The NE-SW fault systems, Nf1-2-3 and Sf1-2-3, displace R1 surface, whereas displacement of Seismo Unit B could be a mimicking effect. For both these fault systems the cumulated R1 displacement is estimated at about 40 m, 20 m for the two easternmost faults Nf3 and Sf3. In proximity of these fault sets R1 is the top erosional surface of the clinoform facies (Figure 6), therefore the activity of these faults can be confined between 50 ka and 10 ka (Seismo Unit B age). A slip rate of about 1.0 mm/yr can therefore be evaluated for Nf1-2-3 and Sf1-2-3 systems. The similarities between these two sets of faults in the northern and southern portions of the basin, both in terms of geometrical arrangement, vertical offset and slip rate, sug-

Fault	Strike	Kinematics	Lenght (km)	Time interval (ka)	Average vertical displacement (m)	Slip rate (mm yr⁻¹)	Average vertical displacement for system (m)	Slip rate for system (mm yr⁻¹)
f1	NE-SW	normal	1.8	-	-	-	-	-
f2	NE-SW	normal	1.3	-	-	-	-	-
f3	NE-SW	normal	1.6	-	-	-	-	-
Nf1	NE-SW	normal	2.5	50-10	10	0.25		
Nf2	NE-SW	normal	2.5	50-10	10	0.25	40	1.0
Nf3	NE-SW	normal	2.5	50-10	20	0.5		
Nf4-L1	ENE-WSW	normal left-lateral strike-slip (?)	5	25 - present	9	~0.4		
Cf1	NNW-SSE	normal	10	25 - present	15	0.6	30 / 35	1.2 / 1.4
Cf2	NNW-SSE	normal	8	25 - present	15 - 20	0.6 - 0.8		
Sf1	NNW-SSE	normal	2.5	50-10	10	0.25		
Sf2	NNW-SSE	normal	3	50-10	10	0.25	40	1.0
Sf3	NNW-SSE	normal	3	50-10	20	0.5	-	-
L2	ENE-WSW	left lateral strike-slip	6.5	25 - present	-	-	-	-
L3	ENE-WSW	left lateral strike-slip	4.5	25 - present	-	-	-	-
L4	ENE-WSW	left lateral strike-slip	3.8	25 - present	-	-	-	-

Table 1. Summary of fault parameters, vertical displacement, age and slip rate of dip-slip fault for different inferred time periods.
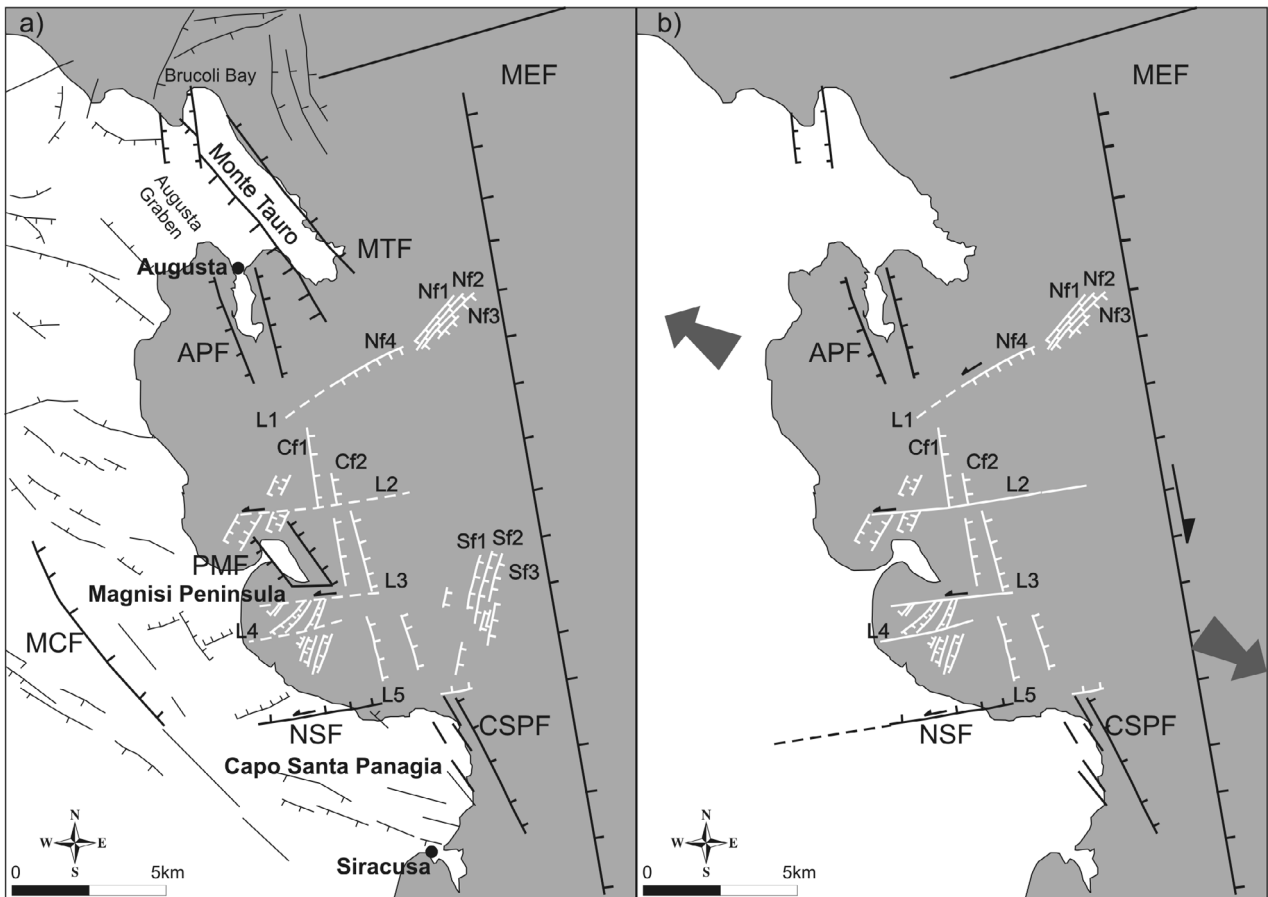
Figure 13. a) Sketch map of the Augusta Basin showing all the faults observed by Chirp profiles, deduced by the morphobathymetric and geomorphological analyses, related to the faults of the entire structural background reported in the literature; b) structural features of the Augusta Basin with active faults observed by Chirp analysis in relation to the APF, NSF and CSPF, of which they may be the likely offshore continuation, and in relation to the MEF (according to Ambrosetti et al. [1987]) of which they are the probable incipient westernmost propagation.

gest that they belong to the same system.

Nf4, Cf1 and Cf2 displace Ms1 and Ms2 surfaces and also involve Seismo Unit B, so we consider these faults as active (Table 1). Moreover, the gas cloud observed in proximity of Nf4 and Cf2 is further evidence of the activity of these faults acting as a preferential emission path [Dingler et al. 2009]. Nf4 cuts Seismo Unit A and also causes seafloor up-warping and active deformation with growth strata geometry into Seismo Unit B. This fault displaces the two marine abrasion surfaces, Ms1 and Ms2 by 9 m in the northern and north-central sectors. Taking into account the vertical displacement of the youngest Ms2, we can deduce a slip rate of 0.4 mm/yr for Nf4 fault starting from 25 ka BP (Table 1). Cf1 displaces the marine abrasion surface Ms2 (25 ka) by about 15 m. Cf2 causes seafloor up-warping, 15 m thickening of Seismo Unit B on its hangingwall and also about 20 m of displacement of the Ms2 surface in the south central and southern sectors. Therefore, we can obtain a slip rate of 0.6 mm/yr for Cf1 and 0.6-0.8 mm/yr for Cf2 since 25 ka. Given their kinematics and location, Cf1 and Cf2 faults probably belong to the same NNW-SSE system that produces almost 30-

35 m of net slip of Ms2, thus the cumulate strain rate for the system is 1.2-1.4 mm/yr.

L2, L3 and L4 lineaments are interpreted as probable left-lateral faults. Similarly, in the northern sector the ~ ENE-WSW trending L1-Nf4, whose vertical slip rate is less than in the other normal faults, could have a left-lateral component. The ENE-WSW trending North Siracusa Fault (Figure 13), bounding the southern Augusta Graben margin [Catalano et al. 2010], could be the southernmost fault belonging to this strike-slip system. f1, f2 and f3 faults delimit extensional basins and develop between the ENE-WSW strike slip structures. Both extensional and strike–slip active faults observed in the Augusta basin are compatible with an inward propagation of extensional-shear deformation occurring along the Malta Escarpment system whose activity is also confirmed by off-shore seismic analysis [Argnani and Bonazzi 2005, Argnani et al. 2012, Firetto Carlino et al. 2012] and by the recent seismicity [Musumeci et al. 2005].

In all, fault kinematics is coherent with the transtensive tectonics characterizing the eastern margin of southern Sicily, confirming that the Ionian domain is

diverging from the Sicilian-Hyblean block (Figure 1) [Palano et al. 2012].

Slip rates are highly variable from fault to fault and, considering the uncertainty on fault activity in space and time, we can only give a rough estimate of the magnitude of associable earthquakes and cannot infer the rupture history of each fault segment. However, according to the empirical relationships obtained by Wells and Coppersmith [1994], the faults we detected in the Augusta Basin, having max length of 10 km, can produce events with magnitude ~ 6.0 and a slip of ~ 0.3 m. Thus these faults are not able to generate earthquakes of magnitude M ~ 7.0, such as the 1169 (M = 6.6) and January 11, 1693, (M = 7.4) events [CPTI Working Group 2004] for which a bigger source is required. Among the offshore faults, the MEF seems to be the best candidate for these events; indeed further away faults such as the STEP Fault, recently proposed by Polonia et al. [2011, 2012], would require very large magnitudes to produce the observed on-land macroseismic reconstructions. The faults observed in the Augusta Basin, being kinematically compatible and geometrically linked with the MEF system can activate when the main fault slips. On the other hand, the observed faults might have generated smaller events that struck the area in the past (e.g. 1848, 1990, 1542 and January 9, 1693) or may have been broken during larger composite events. Indeed, we observe spatial variability in slip rates along the different fault segments. This evidence suggests that the systems ruptured in a complex history, and that if some small earthquakes may be confined to specific segments, larger earthquakes can derive from composite ruptures of fault segments.

Analysis of the two slumped masses observed in the basin (A and B) and involving Holocene sediments (Seismo Unit B) allow relating the slumps to two seismic shaking episodes. Since between the two recorded deformational events, the most recent occurred after 122 BC (the age marked by the tephra layer, Rt) and involved the entire Seismo Unit B above it (Figure 12), the triggering earthquake must have occurred in historical time. Historical data indicate the occurrence of several local earthquakes for this area, thus we can deduce that within the historical time just one event produced sufficiently intense shaking able to generate such effects at the site. Considering the epicentral distance and the magnitude, the best candidate for the triggering event is the January 11, 1693, earthquake. Nonetheless, we cannot exclude that the triggering event was one of the moderate abovementioned shocks. Indeed, moderate earthquakes can trigger slump and sliding off-shore, as secondary effects. The ability of past local earthquakes to generate such deformations in this area is also supported by the presence of seismo-induced features inland, that were associated with the 1693 earthquake and other historical events [Guarnieri et al. 2009, Pirrotta and Barbano 2011, and references therein].

From a tsunami-generation point of view, some authors suggest that large submarine landslides should be considered as the sources of the historical tsunamis that hit this part of the coast after an earthquake [e.g. Billi et al. 2010, Di Bucci et al. 2010]. The Chirp analysis does not cover the total extension of the slumps found in the Augusta Basin but hypothesizing that the real extent of the B body may be twice (2 km^3) the mapped one, it is still not enough to generate a tsunami reproducing the waves observed during the 1693 event. In fact, even a larger 5 km^3 slide, mapped by seismic surveys, more easterly and in rather deep water [Argnani and Bonazzi 2005], modelled by Argnani et al. [2012], is not able to generate the 1693 tsunami. Alternatively, as recently shown for the 1908 tsunami [Favalli et al. 2009] by using the method described by ten Brink et al. [2009], it is possible to explain the effects of the devastating tsunami by assuming that it was caused by coseismic displacement associated with a small-volume landslide, such as that observed in the Augusta basin. However, slumps observed in the Augusta Basin could have triggered the anomalous sea waves locally observed during minor earthquakes [Tinti et al. 2007].

6. Conclusions

The sub-bottom Chirp analysis performed in the Augusta Basin shows stratigraphic and morphological markers of the late Quaternary sea level changes. The oldest, Seismo Unit A, encompasses the Pleistocene bedrock, a falling stage system tract (60-50 ka) and a beach deposit (25 ka). On the Pleistocene bedrock two marine abrasion surfaces 35 ka and 25 ka old were modelled. The youngest Seismo Unit B, represents the Holocene sedimentary sequence.

Furthermore, soft sediment deformations (slumping) involving the Holocene sediments, are found at the foot of some fault scarps and were probably triggered by earthquake shaking.

This Chirp study also highlighted an important structural complexity within the basin with active faults affecting the recent stratigraphic and morphological elements as well.

The parallel NE-SW striking, SE dipping normal faults cropping out near the shelf, seem to be the oldest system and appear inactive since 10 ka. The NNW-SSE striking E dipping extensional fault system shows activity from 25 ka to present. This system is probably dislocated by a ~ ENE-WSW left-lateral strike-slip system that, together with associated extensional dip and

strike-slip structures, seem to be the most recent tectonic elements.

The youngest fault systems, NNW-SSE and ENE-WSW trending, are consistent with the Malta Escarpment Fault of which they can be the westward incipient extension. Also these faults can be the offshore extension of those cropping out inland: the NNW-SSE Brucoli Faults, the ENE-WSW North Siracusa Faults and the Capo Santa Panagia Faults. The ~ ENE-WSW faults seem to be master faults of an extensional shear zone where NE-SW pull-apart structures and extensional strike-slip duplexes branch.

On the basis of their length and kinematics, the observed faults are consistent with the moderate $5 < M < 6$ historical earthquakes that affected eastern Sicily. However, these faults can be geometrically joined to the Malta Escarpment fault and could have moved when the main structure slipped, thereby producing the strongest earthquakes such as the 1169 and the 1693 events. Events of such energy could be responsible of the slumped bodies or they could be triggered by moderate offshore events.

Our results support the hypothesis that the seismogenic sources of southeastern Sicily are located offshore, that the Malta Escarpment is responsible for part of the regional seismicity and that it could represent the lithospheric boundary between the Sicilian-Hyblean and Ionian blocks across which they are diverging.

Moreover Chirp data on slumped masses can further be exploit to assess tsunami hazard in the area, using relationships between submarine landslides and earthquakes.

References

Adam, J., C.D. Reuther, M. Grasso and L. Torelli (2000). Active fault kinematics and crustal stresses along the Ionian margin of southeastern Sicily, Tectonophysics, 326, 217-239.

Alsop, G.I., and S. Marco (2011). Soft-sediment deformation within seismogenic slumps of the Dead Sea Basin, J. Struct. Geol., 33, 433-457.

Amato, A., R. Azzara, A. Basili, C. Chiarabba, M. Cocco, M. Di Bona and G. Selvaggi (1995). Main shock and aftershocks of the December 13, 1990, eastern Sicily earthquake, Annali di Geofisica, 38 (2), 255-266.

Ambrosetti, P., C. Bosi, F. Carraro, N. Ciaranfi, M. Panizza, G. Papani, L. Vezzani and A. Zanferrari (1987). Neotectonic map of Italy; scale 1:500.000, Sheet 6 (Calabria meridionale e Sicilia), L.A.C., Firenze.

Argnani, A., and C. Bonazzi (2005). Malta Escarpment fault zone offshore eastern Sicily: Pliocene- Quaternary tectonic evolution based on new multichannel aseismic data, Tectonics, 24, TC4009, 1-12.

Argnani, A., A. Armigliato, G. Pagnoni, F. Zaniboni, S. Tinti and C. Bonazzi (2012). Active tectonics along the submarine slope of south-eastern Sicily and the source of the 11 January 1693 earthquake and tsunami, Nat. Haz. Earth Syst. Scie., 12, 1-9.

Argnani, A., F. Mazzarini, C. Bonazzi, M. Bisson and I. Isola (2013). The deformation offshore of Mount Etna as imaged by multichannel seismic reflection profiles, J. Volcanol. Geoth. Res., 251, 50-64.

Azzaro, R., and M. S. Barbano (2000). Analysis of the seismicity of Southeastern Sicily: a proposed tectonic interpretation, Annali di Geofisica, 43 (1), 171-188.

Basili, R., G. Valensise, P. Vannoli, P. Burrato, U. Fracassi, S. Mariano, M.M. Tiberti and E. Boschi (2008). The Database of Individual Seismogenic Sources (DISS), version 3: summarizing 20 years of research on Italy's earthquake geology, Tectonophysics, 453, 20-43.

Bianca, M., C. Monaco, L. Tortorici and L. Cernobori (1999). Quaternary normal faulting in southeastern Sicily (Italy): a seismic source for the 1693 large earthquake, Geophys. J. Int., 139, 370-394.

Billi, A., L. Minelli, B. Orecchio and D. Presti (2010). Constraints to the Cause of Three Historical Tsunamis (1908, 1783, and 1693) in the Messina Straits Region, Sicily, Southern Italy, Seismol. Res. Lett., 81(6), 907-915.

Brancato, A., J.A. Hole, S. Gresta and J.N. Beale (2009). Determination of Seismogenic Structures in Southeastern Sicily (Italy) by High-Precision Relative Relocation of Microearthquakes, Bull. Seismol. Soc. Am., 99, 3, 1921-1936.

Bull, J.M., P.M Barnes., G. Lamarche, D.J. Sanderson, P.A. Cowie, S.K. Taylor and J.K. Dix (2006). High-resolution record of displacement accumulation on an active normal fault: implications for models of slip accumulation during repeated earthquakes, J. Struct. Geol., 28, 1146-1166.

Carbone, S., ed. (2011). Carta Geologica d'Italia, Foglio 641: Augusta, scale 1:50,000, Servizio Geologico d'Italia and Regione Siciliana, S.EL.CA, Firenze.

Carter, L. (2012). Acoustical characterisation of seafloor sediments and its relationship to active sedimentary

processes in Cook Strait, New Zealand, New Zealand J. Geol. Geophys., 35 (3), 289-300.

Catalano, S., G. Romagnoli and G. Tortorici (2010). Kinematics and dynamics of the Late Quaternary rift-flank deformation in the Hyblean Plateau (SE Sicily), Tectonophysics, 486, 1-14.

Chiarabba, C., P. De Gori and F. Speranza (2008). The southern Tyrrhenian subduction zone, Deep geometry, magmatism and Plio-Pleistocene evolution, Earth Plan. Scie. Letters, 268, 408-423.

CPTI Working group (2004). Catalogo Parametrico dei Terremoti Italiani, versione 2004 (CPTI04), INGV, Bologna; http://emidius.mi.ingv.it/CPTI/.

Dewey, J.F., M.L. Helman, E. Turco, D.H.W. Hutton and S.D. Knott (1989). Kinematics of the Western Mediterranean, In: M.P. Coward, D. Dietrich and R.G. Park (eds.), Alpine tectonics, Geol. Soc. London, Special Publications, 45, 265-283.

Di Bucci, D., P. Burrato, P. Vannoli and G. Valensise (2010). Tectonic evidence for the ongoing Africa-Eurasia convergence in central Mediterranean fore-land areas: A journey among long-lived shear zones, large earthquakes, and elusive fault motions, J. Geoph. Res. Solid Earth, 115 (12), B12404.

Di Grande, A., and G. Scamarda (1973). Segnalazione di livelli a Strombus bubonius Lamarck nei dintorni di Augusta (Siracusa), Boll. Acc. Gioenia Scie. Nat., ser. 4, 11 (9-10), 157-172.

Dingler, J., G. Kent, N. Driscoll, J. Babcock, A. Harding, G. Seitz, B. Karlin and C. Goldman (2009). A high-resolution seismic CHIRP investigation of active normal faulting across Lake Tahoe Basin, California-Nevada, Geol. Soc. Am. Bull., 121 (7-8), 1089-1107.

DISS Working Group (2010). Database of Individual Seismogenic Sources (DISS), Version 3.1.1: A compilation of potential sources for earthquakes larger than M 5.5 in Italy and surrounding areas. http://diss.rm.ingv.it/diss/, © INGV 2010, Istituto Nazionale di Geofisica e Vulcanologia.

Doglioni, C., E. Carminati, M. Cuffaro and D. Scrocca (2007). Subduction kinematics and dynamic constraints, Earth-Science Reviews, 83, 125-175.

Doughty, M., N. Eyles and L. Daurio (2010). Earthquake (1935 Timiskaming M6.2) triggered slumps in Lake Kipawa, Western Quebec Seismic Zone, Canada, Sedim, Geol., 228, 113-118.

Favalli, M., E. Boschi, F. Mazzarini and M.T. Pareschi (2009). Seismic and landslide source of the 1908 Straits of Messina tsunami (Sicily, Italy), Geoph. Res. Letters, 36, L16304; doi:10.1029/2009GL039135).

Finetti, I.R., and A. Del Ben (1996). Crustal Tectono-Stratigraphic Setting of the Pelagian Foreland from New CROP Seismic Data, In: I.R. Finetti (ed.), CROP PROJECT, Deep Seismic Exploration of the Central Mediterranean and Italy, 26, 581-595.

Firetto Carlino, M., A. Di Stefano and F. Budillon (2012). Seismic facies and seabed morphology in a tectonically controlled continental shelf: The Augusta Bay (offshore eastern Sicily, Ionian Sea), Mar. Geol., 335, 35-51.

Gasperini, L., and G. Stanghellini (2009). SEISPRHO: an interactive computer program for processing and interpretation of high-resolution seismic reflection profiles, Computers and Geosciences, 35, 1497-1507.

Guarnieri, P., C. Pirrotta, M.S. Barbano, P. M. De Martini, D. Pantosti, F. Gerardi and A. Smedile (2009). Paleoseismic investigation of historical liquefaction along the Ionian coasts of Sicily, J. Earthq. Eng., 13, 68-79.

Hunt, D., and M.E. Tucker (1992). Stranded parasequences and the forced regressive wedge system tract: deposition during base level fall, Sediment. Geol., 81, 1-9.

Istituto Idrografico della Marina (1999). Carta Nautica da Capo Passero a Capo S. Croce, scala 1:100.000.

Lajoie, K.R., D.J. Ponti, C.L. Powell, S.A. Mathieson, and A.M. Sarna-Wojcicki (1991). Emergent marine strandlines and associated sediments, coastal California: a record of Quaternary sea-level fluctuations, vertical tectonic movements, climatic changes and coastal processes, in: R.B. Morrison (ed.), Quaternary Non-Glacial Geology: Conterminous United States, Geological Society of America Decade of North America Geology, K-2, 190-214.

Le Dantec, N., L.J. Hogarth, N.W. Driscoll, J.M. Babcock, W.A. Barnhardt and W.C. Schwab (2010). Tectonic controls on nearshore sediment accumulation and submarine canyon morphology offshore La Jolla, Southern California, Mar. Geol., 268, 115-128.

Lentini, F., and L. Vezzani (1978). Tentativo di elaborazione di uno schema strutturale della Sicilia orientale, Mem. Soc.Geol. It., 19, 495-500.

Monaco, C., and Tortorici L. (2000). Active faulting in the Calabrian arc and eastern Sicily, J. Geodynamics, 29, 407-424.

Musumeci, C., D. Patanè, L. Scarfì and S. Gresta (2005). Stress directions and shear-wave anisotropy: observations from local earthquakes in southeastern Sicily, Italy, Bull. Seismol. Soc. Am., 95 (4), 1359-1374.

Nummedal, D., and D.J.P. Swift (1987). Transgressive stratigraphy at sequence-bounding unconformities: some principles derived from Holocene and Cretaceous examples, In: D. Nummedal, O.H. Pilkey and J.D. Howard (eds.), Sea-level fluctuation and coastal evolution, Society Economic Paleontologists Mineralogists, S.P. 4, 241-260.

Palano, M., L. Ferranti, C. Monaco, M. Mattia, M. Aloisi, V. Bruno, F. Cannavò and G. Siligato (2012). GPS velocity and strain fields in Sicily and southern Calabria, Italy: Updated geodetic constraints on tectonic block interaction in the central Mediterranean, J. Geophys. Res., 117, B07401.

Peacock, D.C.P., and D.J. Sanderson (1995). Strike-slip relay ramps. J. Struct. Geol., 17, 1351-1360.

Pirrotta, C., and M.S. Barbano (2011). Analysis of deformation structures in Pliocene and Quaternary deposits of the Hyblean Plateaux (South-eastern Sicily), Tectonophysics, 499, 41-53.

Polonia, A., L. Torelli, P. Mussoni, L. Gasperini, A. Artoni and D. Klaeschen (2011). The Calabrian Arc subduction complex in the Ionian Sea: Regional architecture, active deformation, and seismic hazard, Tectonics, 30, TC5018.

Polonia, A., L. Torelli, L. Gasperini and P. Mussoni (2012). Active faults and historical earthquakes in the Messina Straits area (Ionian Sea), Natural Hazards and Earth System Sciences, 12, 2311-2328; doi:10.5194/nhess-12-2311-2012.

Rebesco, M., R.C. Neagu, A. Cuppari, F. Muto, D. Accettella, R. Dominici, A. Cova, C. Romano and A. Caburlotto (2009). Morphobathymetric analysis and evidence of submarine mass movements in the western Gulf of Taranto (Calabria margin, Ionian Sea), Int. J. Earth Sciences (Geol Rundsch), 98, 791-805.

Sagnotti, L., A. Smedile, P.M. De Martini, D. Pantosti, F. Speranza, A Winkler., P. Del Carlo, L.G. Bellucci and L. Gasperini (2011). A continuous palaeosecular variation record of the last four millennia from the Augusta Bay (Sicily, Italy), Geophys. J. Int., 184, 191-202.

Scandone, P., E. Patacca, R. Radoicic, W.B.F. Ryan, M.B. Cita, M. Rawson, H. Chezar, E. Miller, J. Mckenzie and S. Rossi (1981). Mesozoic and Cenozoic rocks from Malta Escarpment (Central Mediterranean), Am. Ass. Petroleum Geologists Bull., 65, 1299-1319.

Smedile, A., P.M. De Martini, D. Pantosti, L. Bellucci, P. Del Carlo, L. Gasperini, C. Pirrotta, A. Polonia and E. Boschi (2011). Possible tsunami signatures from an integrated study in the Augusta Bay offshore (Eastern Sicily-Italy), Mar. Geol., 281, 1-13.

ten Brink, U.S., H. J. Lee, E.L. Geist and D. Twichell (2013). Assessment of tsunami hazard to the U.S. East Coast using relationships between submarine landslides and earthquakes, Mar. Geol., 264, 65-73.

Tinti, S., A. Maramai and L. Graziani (2007). The Italian Tsunami Catalogue (ITC), Version 2, Available at: http://www.ingv.it/servizi-e-risorse/BD/catalogo-tsunami/catalogo-degli-tsunami-italiani.

Visini, F., R. De Nardis, M.S. Barbano and G. Lavecchia (2009). Testing the seismogenic sources of the January 11th 1693 Sicilian earthquake (Io X/XI): some insights from macroseismic field simulations, Boll. Soc. Geol. It., 128 (1), 147-156.

Wells, D.L., and K.J. Coppersmith (1994). New empirical relationship among magnitude, rupture length, rupture width, rupture area, and surface displacement, Bull. Seismol. Soc. Am., 84 (4), 974-1002.

*Corresponding author: Claudia Pirrotta,
Università di Catania, Dipartimento di Scienze Biologiche, Geologiche e Ambientali, Catania, Italy;
email: c.pirrotta@unict.it, claudiapirrotta@hotmail.com.